Light Metals 2013 *Edited by: Barry Sadler*
TMS (The Minerals, Metals & Materials Society), 2013

ON THE AGING BEHAVIOR OF AA2618 DC CAST ALLOY

P. Shen, E.M. Elgallad, X.-G. Chen

University of Quebec at Chicoutimi, Saguenay, QC, Canada, G7H 2B1

Keywords: AA2618 aluminum alloy, DC cast ingot, aging behavior, microstructure, electrical conductivity, DSC analysis

Abstract

Due to their excellent mechanical properties and dimension stability, Direct Chill (DC) cast ingot plates of AA2618 alloy have been increasingly used for manufacturing large molds. The microstructure of the AA2618 DC cast alloy was examined in as-cast and solution-treated conditions using optical and scanning electron microscopes. The aging behavior of the non-deformed alloy at artificial and natural aging conditions was studied. The precipitation characteristics of the alloy were studied by differential scanning calorimetry and electrical conductivity measurement. The peak-aged conditions of the alloy were attained after aging for 36 h at 175ºC, 10 h at 195ºC, and 1 h at 215ºC with hardness values of 99, 97, and 95 HRF respectively. It was found that the strengthening mechanisms of the natural and artificial aging were differently controlled by the formation of Cu-Mg co-clusters and/or GPB zones and *S*-Al_2CuMg phase respectively.

Introduction

AA2618 is an Al-Cu-Mg alloy containing a certain amount of Fe and Ni, where Cu and Mg contribute to the strengthening through age hardening, whereas Fe and Ni provide dispersion hardening and also assist in stabilizing the microstructure by forming Fe and Ni intermetallic compounds. This alloy was originally designated as a wrought alloy to be used after undergoing hot deformation processes such as forging and rolling. It is capable of developing a combination of medium-high strength and good ductility while retaining its strength at relatively high temperatures of up to 300°C [1]. In recent years, Direct Chill (DC) cast ingot plates of the AA2618 alloy have been increasingly used for manufacturing large molds, such as low and high pressure injection molds in the plastic industry as well as prototype molds in the automotive industry, due to their excellent mechanical properties and dimensional stability. To meet the extremely large mold dimension requirements, the large plates are cut directly from the DC cast ingots and used in the non-deformed condition, which can significantly reduce the manufacturing steps and production costs.

The 2xxx (Al-Cu-Mg) series alloys are the most commonly used age-hardenable aluminum alloys. In these alloys, the nature of the precipitation strengthening phases during the aging process depends on the Cu/Mg ratio. The general precipitation sequence in the Al-Cu-Mg alloys with a Cu/Mg weight ratio ≥ 2.2:1 was proposed as follows: supersaturated solid solution (SSSS) → GPB zones → *S*'' → *S*' → *S* [2]. Bagaryatsky [2] considered the GPB zone as a short-range ordering of Cu and Mg solute atoms. The equilibrium phase *S*-Al_2CuMg has been determined as an orthorhombic structure with lattice parameters identified as a = 0.400 nm, b = 0.923 nm, c = 0.714 nm [3]. However, the structure of *S*'' has not been clearly confirmed. The *S*' phase has generally been considered as semi-coherent with the matrix. As the *S*' phase possesses the same structure as the *S* phase but with a slight difference in the lattice parameters, it is now considered that there is no distinction between these two phases [4, 5].

The use of an atom probe field ion microscope and a three-dimensional atom-probe proves that the initial age hardening is due to the formation of co-clusters [6, 7]. Ringer *et al.* [8] proposed the following 3-stage precipitation sequence for the aging of Al–Cu–Mg alloys: SSSS → Cu-Mg co-clusters → GPB zone → *S*, where the Cu–Mg co-clusters are responsible for the initial hardening. The GPB zone is the dominant precipitate at peak strengthening and the *S* phase appears in the softening stage. However, Gao *et al.* [9] and Wang *et al.* [4] found that the peak aging was dominated by the formation of *S* phase precipitates and no significant amounts of other phases or zones were detected. However, information concerning the microstructural evolution during natural aging is scarce. Starink [7] found that the strengthening due to the modulus hardening generated by the difference in shear modulus of the Cu–Mg co-clusters and the matrix is the main strengthening mechanism for room temperature hardening of Al-Cu-Mg alloys. Based on the results of natural aging in laboratory Al–Cu–(Mg) alloys and in the AA2024 alloy, Klobes *et al.* [10] concluded that the natural aging hardening process was associated with the growth of co-clusters and that no *S*'' phase formed during the natural aging of the investigated alloys.

As previously mentioned, the AA2618 alloy was designated as a wrought alloy and many works were centered on the deformed alloy conditions. To date, the aging behavior of the AA2618 alloy has not yet been studied in the non-deformed condition. The present study was therefore conducted with the intention of understanding the aging behavior of the non-deformed AA2618 DC cast alloy by using a series of characterization techniques including hardness testing, DSC analysis, and electrical conductivity measurement.

Experimental Procedure

The material used in this study was a 50 mm thick transverse slice cut from a large industrial AA2618 DC cast ingot. The chemical composition of the alloy is listed in Table 1. Test specimens were cut from the cross-section slice for heat treatment, metallographic examination, DSC analysis and electrical conductivity measurement. The solution treatment was carried out at 530°C for 5 h, followed by water quenching at room temperature. Artificial and natural aging treatments were subsequently carried out at 175, 195 and 215 °C for times ranging from 1 to 110 h, and at room temperature for durations of 10 h to 5 weeks, respectively. All heat treatments were conducted in a forced-air electric furnace.

Table 1 Chemical composition (wt. %) of AA2618 alloy used

Cu	Mg	Fe	Ni	Si	Zn	Ti	Mn	Al
2.86	0.97	0.97	1.04	0.14	0.10	0.02	<0.01	Bal.

The microstructures of as-cast and solution-treated samples were examined using an optical microscope and a scanning electron microscope (SEM, JEOL JSM-6480LV) equipped with an energy dispersive X-ray spectrometer (EDX). A Rockwell hardness test (scale F) was performed on as-quenched and aged samples. Six indentations were made on each sample and the average hardness value was reported. Electrical conductivity measurements were conducted on ground and polished samples using a portable electrical conductivity measurement system (FISCHER SIGMASCOPE SMP 10). The change in the electrical conductivity was measured at room temperature in terms of percentage of the international annealed copper standard (%IACS). As-cast and heat-treated samples were analyzed using a computerized differential scanning calorimeter (PerkinElmer DSC8000). The weight of the DSC sample was approximately 20 mg and the heating rate was fixed at 10°C/min. A protective gas atmosphere of pure argon was applied.

Results and Discussion

Microstructure

The micrographs shown in Figure 1 display the microstructure of the as-cast AA2618 alloy. It can be observed that the as-cast structure consists of four major coarse intermetallic phases, namely Al_2Cu, Al_7Cu_4Ni, $Al_7Cu_2(Fe,Ni)$ and Al_9FeNi distributed in the interdendritic regions, as well as fine Al_2CuMg particles dispersed in the α-Al matrix.

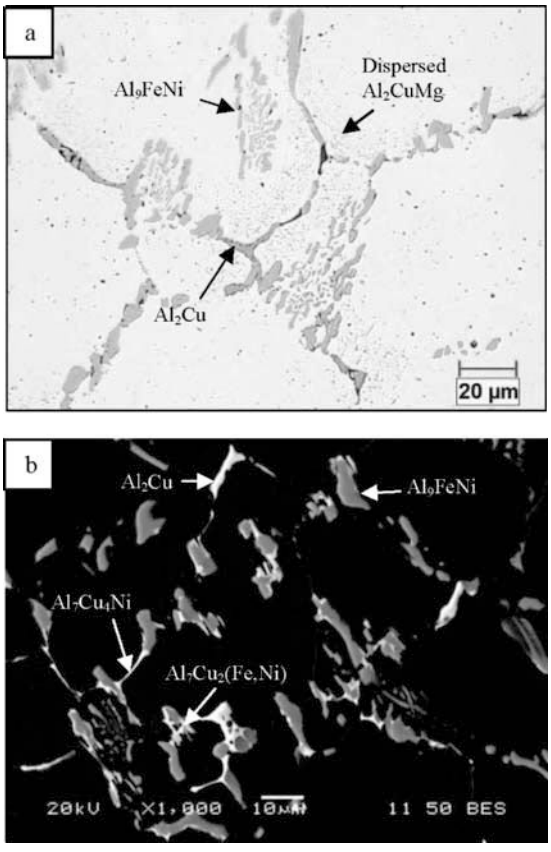

Figure 1 Microstructure of the as-cast AA2618 alloy: (a) optical and (b) SEM backscattered micrographs.

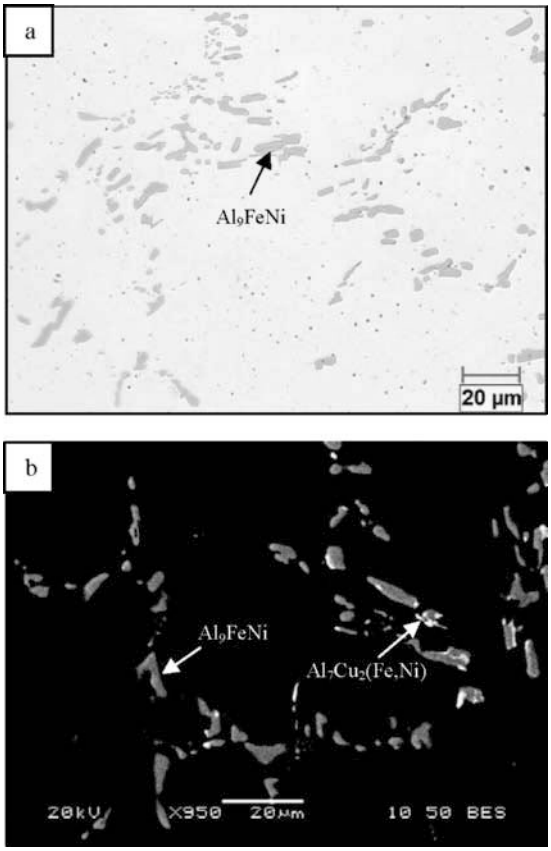

Figure 2 Microstructure of the solution-treated AA2618 alloy: (a) optical and (b) SEM backscattered micrographs.

The effect of solution treatment on the alloy microstructure is shown in Figure 2. It is evident that the Al_2Cu, Al_2CuMg and Al_7Cu_4Ni phases were almost completely dissolved in the α-Al solid solution after the solution treatment. On the other hand, the $Al_7Cu_2(Fe,Ni)$ and Al_9FeNi phases could not be dissolved and were only subjected to fragmentation and spheroidization.

Figure 3 shows the DSC heating curves of the AA2618 alloy in the as-cast and solution treated conditions. The DSC curve of the as-cast alloy exhibits six endothermic peaks at 508.3, 539.9, 553.4, 575.5, 634.0 and 646.5°C, respectively. The first peak at 508.3°C represents the low melting point of the Al_2CuMg phase precipitated by a quaternary eutectic reaction at the last stage of solidification. The second peak at 539.9°C is attributed to the melting of the block-like Al_2Cu phase. The following three peaks are related to the melting of the Fe and Ni intermetallic phases, namely Al_7Cu_4Ni, $Al_7Cu_2(Fe,Ni)$ and Al_9FeNi, respectively. The last large peak corresponds to the bulk melting of the primary α-Al. The DSC curve of the solution-treated alloy is in line with the microstructural observations. It is apparent that the first three peaks disappeared, which indicates that the Al_2CuMg, Al_2Cu, and Al_7Cu_4Ni phases were dissolved into the solid solution. The two subsequent peaks, corresponding to the melting of the $Al_7Cu_2(Fe,Ni)$ and Al_9FeNi phases which were not dissolved by the solution treatment, still appear on the DSC curve.

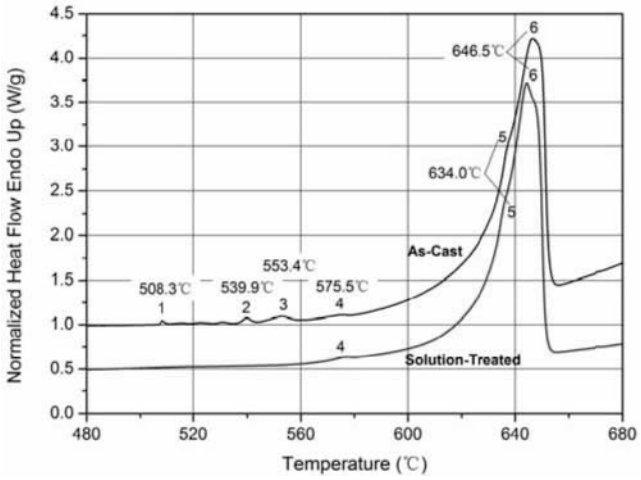

Figure 3 DSC heating curves of AA2618 samples in as-cast and solution-treated conditions.

Aging behavior

Figure 4a shows the hardness values of the AA2618 alloy as a function of the aging temperature and time. It can be observed that the maximum hardness of 99 HRF was obtained after 36 h of aging at 175°C. Increasing the aging temperature to 195°C shortened the time to reach the peak hardness to 10 h. However, the peak hardness value was slightly decreased to 97 HRF. It is interesting to note that for both aging conditions at 175 and 195°C, the hardness of the AA2618 alloy tends to decrease slowly after reaching peak hardness, contrary to the Al-Cu binary alloys [11]. This observation indicates that the AA2618 alloy is not very susceptible to overaging with increasing time, which may be due to the low coarsening tendency of its main strengthening phase, *S*-Al_2CuMg [12, 13]. Aging at 215°C further shortened the time to peak hardness to 1 h. This aging condition achieved a peak hardness value (95 HRF) slightly lower than that obtained by aging at 195°C. Prolonged aging at 215°C beyond 4 h seemed to lead to a rapid decline in the hardness as compared to aging conditions at 175 and 195°C.

The natural aging behavior of the AA2618 alloy was also investigated by aging alloy samples at room temperature for aging times ranging from 10 h to 5 weeks. The corresponding curve, as illustrated in Figure 4b, reveals that the AA2618 alloy has a high tendency to natural aging. As can be observed, the hardness increased rapidly from 75 to 90 HRF during the first 24 h, and then gradually increased, to 94 HRF after 3 weeks. Prolonged natural aging beyond 3 weeks did not cause any significant change in the hardness values and an almost constant plateau was obtained. It is worthwhile noticing that the peak hardness value obtained by natural aging is comparable to the peak hardness values achieved after artificial aging at 195 and 215°C.

Precipitation Characteristics

Electrical Conductivity Measurement. Figure 5a shows the variation in the electrical conductivity of the AA2618 alloy as a function of aging time at different isothermal holding temperatures. The value of the electrical conductivity in the as-quenched condition, was found to be 35.9 %IACS. It is obvious that except for the initial slight decrease at 175°C, the electrical conductivity increased with increasing aging temperature and extending aging time. The increasing rates of the electrical conductivity at higher aging temperatures (195 and 215°C) were higher than at a lower temperature (175°C), which is ascribed to the faster precipitation process at higher temperatures. During the overaging stages at 195 and 215°C beyond 10 and 1 h respectively, the electrical conductivity increased very slowly and became constant, indicating that the supersaturation degree of the solid solution had been greatly reduced. However, the increasing rate of the electrical conductivity at 175°C after 36 h only declined slightly, indicating that there was still a considerable amount of solute atoms existing in the solid solution even after reaching peak aging. Contrary to the artificial aging, the electrical conductivity of the AA2618 alloy decreased at the beginning of the natural aging and then became idle to change when increasing the aging time and displayed an almost constant value, as shown in Figure 5b.

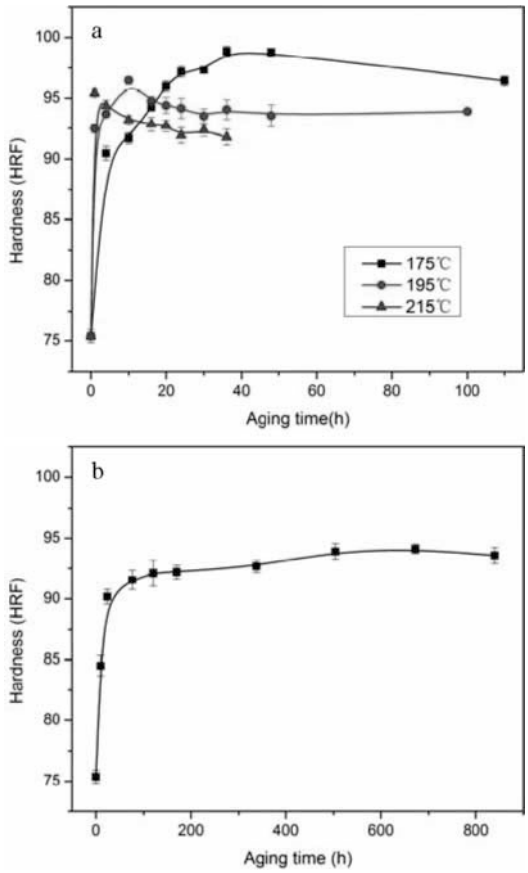

Figure 4 Age-hardening behavior of AA2618 alloy: (a) artificial aging at 175, 195 and 215 °C, and (b) natural aging at room temperature.

The decrease in the electrical conductivity of the AA2618 alloy during the first few hours of the artificial aging at 175°C and after the natural aging, is possibly due to the formation of GPB zones [14]. The effective scattering of electrons by the evenly dispersed GPB zones leads to an increase in the electrical resistance and is a decrease in the electrical conductivity [15]. The increase in the electrical conductivity during the artificial aging can be explained in terms of the progressive reduction in the degree of supersaturation of the α-Al solid solution by solute atoms [14, 16].

The solute atoms of Cu and Mg, which act as scatterers of electrons, precipitate out of the aluminum matrix by forming *S* phase. In contrast with the GPB zones, the relatively large *S* phase precipitates scatter electrons to a lesser degree. The conductivity at 195 and 215°C attains the ultimate value of 45 % IACS, at which time the Cu and Mg atoms have been fully precipitated out of the solid solution.

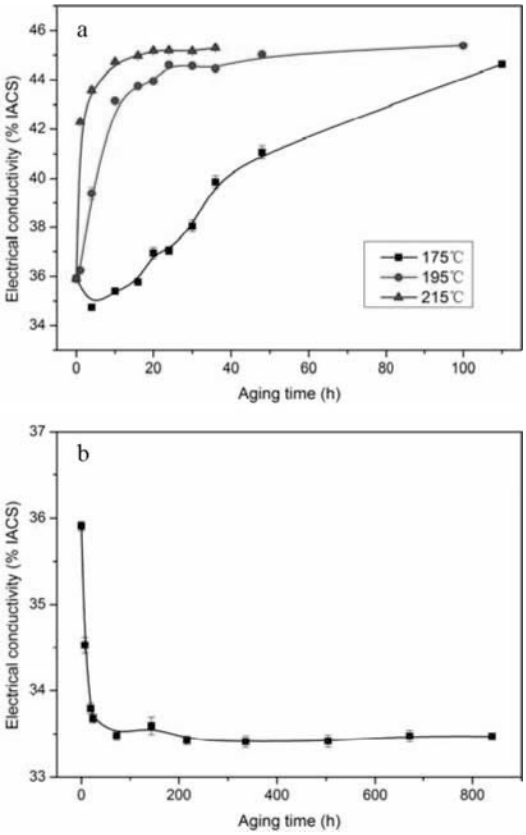

Figure 5 Electrical conductivity vs. aging time curves of the AA2618 alloy: (a) artificial aging at different temperatures, and (b) natural aging at room temperature.

DSC analysis. To understand the microstructural changes during the artificial and natural aging which cause the hardness and electrical conductivity variations, DSC analysis was performed on as-quenched and aged AA2618 alloy samples. Figure 6a shows the DSC thermograms of the AA2618 alloy in the as-quenched and different artificial aging conditions. Three main peaks may be identified in these thermograms [4, 9]: an endothermic peak B between 180 and 240°C, attributed to the dissolution of the GPB zone; an exothermic peak C between about 240 and 320°C, representing the formation of *S* phase precipitates, and a broad endothermic peak D between 340 and 480°C, corresponding to the progressive dissolution of the *S* precipitates [7]. The DSC curve of the as-quenched alloy displays the largest heat effect for the exothermic peak C, indicating the highest degree of supersaturation of the α-Al solid solution by solute atoms, which transform to *S*-phase during the DSC heating run. For the artificial aging at 195°C, both the dissolution peak of the GPB zones and the formation peak of the *S* phase decrease with extended aging time. This means that the samples aged for a longer period contained less GPB zones and more S phase precipitates, that is, more GPB zones were transformed to the main strengthening contributor *S* phase [4]. At the peak aging (195°C for 10 h) and overaging (195°C for 36 h) conditions, the *S* phase formation peak almost disappeared. These observations imply that the artificial age-hardening of the AA2618 alloy is mainly ascribed to the progressive precipitation of the *S* phase, which forms dense *S*-Al_2CuMg precipitates at the peak hardness stage.

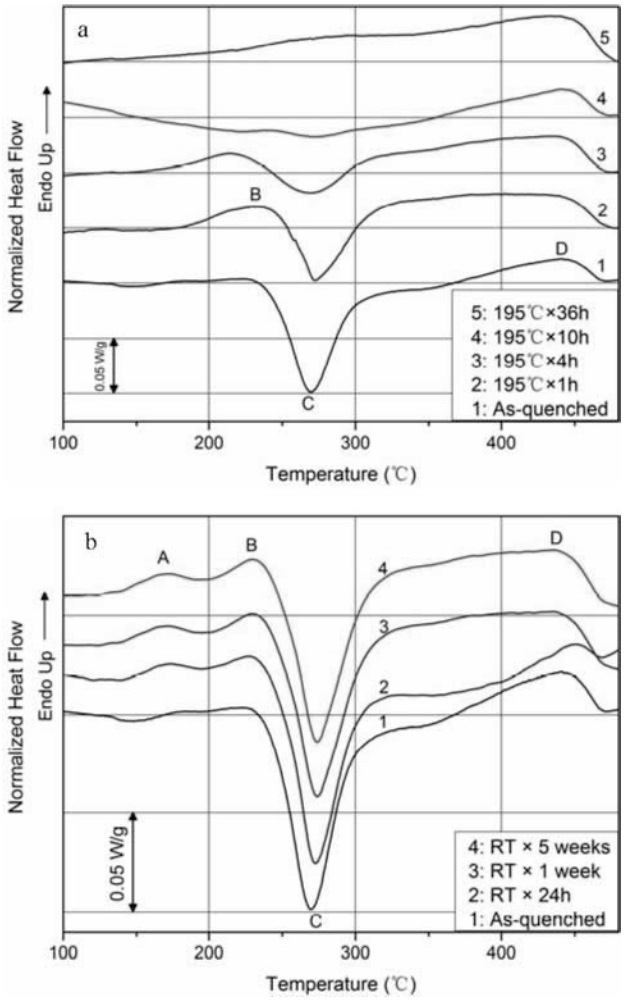

Figure 6 DSC thermograms of the AA2618 alloy in: (a) as-quenched and artificial aging conditions, and (b) as-quenched and natural aging conditions (RT refers to room temperature).

Figure 6b shows the DSC thermograms of the AA2618 alloy in the as-quenched and different natural aging conditions. Besides the three peaks observed in the artificial-aged samples, another endothermic peak A between 150 and 180°C temperature range is identified and may be attributed to the dissolution of Cu and Mg co-clusters. Due to the slow precipitation speed and low temperature during natural aging, the precipitated co-clusters could be retained, while this could hardly be found during the artificial aging process. The DSC curves also revealed that the dissolution peaks B of the co-clusters and GPB zones increase with extended aging time. On the other hand and compared to the as-quenched sample, the formation peak C of the *S* phase has only a slight decline after a prolonged natural aging time of up to 5 weeks, indicating that the *S* phase is rarely formed during natural

aging. These observations suggest that the natural age-hardening of the AA2618 alloy is dominated by the co-clusters and GPB zones. It is obvious that the DSC analysis is consistent with the electrical conductivity measurement with respect to the precipitation characteristics of the AA2618 alloy in both artificial and natural aging conditions.

In future works, results of the DSC analysis for the precipitation characteristics will be verified by TEM observations.

Conclusions

An investigation was carried out on the aging behavior of the AA2618 DC cast alloy that is directly used for the manufacturing of large molding plates. Based on the results obtained, the following conclusions can be drawn:

(1) The peak-aged conditions of the AA2618 DC cast alloy were attained after aging for 36 h at 175°C, 10 h at 195°C, and 1 h at 215°C with hardness values of 99, 97 and 95 HRF respectively.

(2) The AA2618 DC cast alloy was found to be prone to natural aging, displaying hardness values comparable to those obtained by artificial aging at 195 and 215°C.

(3) The electrical conductivity of the AA2618 alloy decreased during the first 4 h of aging at 175°C and during the whole natural aging process due to the formation of GPB zones; the electrical conductivity increased over most artificial aging periods, due to the reduction of supersaturation of solid solution.

(4) Based on the results of the electrical conductivity measurement and the DSC analysis, it is suggested that under artificial aging, the main strengthening phase of the AA2618 DC cast alloy is *S*-Al_2CuMg phase, whereas the strengthening effect caused by the natural aging is mainly attributed to the formation of Cu-Mg co-clusters and/or GPB zones.

Acknowledgements

The authors would like to acknowledge the financial support from PCP Canada, the Fonds de recherche sur la nature et les technologies (FQRNT) and the Natural Sciences and Engineering Research Council of Canada (NSERC). The authors also would like to thank PCP Canada for providing the DC cast ingot materials and the technical support.

References

1. I. Özbek, "A study on the re-solution heat treatment of AA 2618 aluminum alloy," *Materials Characterization,* 58 (2007), 312-317.
2. Y.A. Bagaryatsky, "Structural changes on aging Al-Cu-Mg alloys," *Dokl. Akad. Nauk SSSR,* 87 (1952), 397-401.
3. H. Perlitz, and A. Westgren, "The crystal structure of Al_2CuMg," *Ark. Kemi, Mineral. Geol.,* 16 B (1943), 1-5.
4. S.C. Wang, M.J. Starink, and N. Gao, "Precipitation hardening in Al-Cu-Mg alloys revisited," *Scripta Materialia,* 54 (2006), 287-291.
5. S.C. Wang, and M.J. Starink, "Two types of S phase precipitates in Al-Cu-Mg alloys," *Acta Materialia,* 55 (2007), 933-941.
6. S.P. Ringer et al., "Cluster hardening in an aged Al-Cu-Mg alloy," *Scripta Materialia,* 36 (1997), 517-521.
7. M.J. Starink, N. Gao, and J.L. Yan, "The origins of room temperature hardening of Al-Cu-Mg alloys," *Materials Science and Engineering a-Structural Materials Properties Microstructure and Processing,* 387 (2004), 222-226.
8. S.P. Ringer, S.K. Caraher, and I.J. Polmear, "Response to comments on cluster hardening in an aged Al-Cu-Mg alloy," *Scripta Materialia,* 39 (1998), 1559-1567.
9. N. Gao et al., "Precipitation in stretched Al-Cu-Mg alloys with reduced alloying content studied by DSC, TEM and atom probe," *Aluminum Alloys 2002: Their Physical and Mechanical Properties Pts 1-3,* ed. P. J. Gregson and S. J. Harris (Zurich-Uetikon: Trans Tech Publications Ltd, 2002), 923-928.
10. B. Klobes, K. Maier, and T.E.M. Staab, "Natural ageing of Al–Cu–Mg revisited from a local perspective," *Materials Science and Engineering: A,* 528 (2011), 3253-3260.
11. H.K. Hardy, "The Ageing Characteristics of Binary Aluminium-Copper Alloys," *Journal of the institute of metals,* 79 (1951), 321-369.
12. W. Rainforth, and H. Jones, "Coarsening of S'-Al2CuMg in Al-Cu-Mg base alloys," *Journal of Materials Science Letters,* 16 (1997), 420-421.
13. L.M. Rylands, W.M. Rainforth, and H. Jones, "Coarsening rates of S' precipitates in Al-4.1wt% Cu-1.6wt% Mg alloy during extended treatment at 200 °C," *Philosophical Magazine Letters,* 76 (1997), 63-67.
14. M. Rosen et al., "The aging process in aluminum alloy 2024 studied by means of eddy currents," *Materials Science and Engineering,* 53 (1982), 191-198.
15. P.L. Rossiter, and P. Wells, "The electrical resistivity during pre-precipitation processes," *Philosophical Magazine,* 24 (1971), 425-436.
16. C. Panseri, and T. Federighi, "A resistometric study of pre-precipitation in Al-10% Zn," *Acta Metallurgica,* 8 (1960), 217-238.